USING DIC TO MEASURE DEFORMATION FIELDS OF CONCRETE MASONRY TEST SPECIMENS

Prashanth A. Vanniamparambil[1], Fuad Khan[2], Eric Schwartz[1], Antonios Kontsos[3], Ivan Bartoli [4], Mohammad Bolhassani[2], Ahmad Hamid[4]

[1] Graduate students, Department of Mechanical Engineering and Mechanics, Drexel University, Philadelphia, PA 19104, USA

[2] Graduate student, Department of Civil, Architectural and Environmental Engineering, Drexel University, Philadelphia, PA 19104, USA

[3]Assistant Professor, Department of Mechanical Engineering and Mechanics, Drexel University, Philadelphia, PA 19104, USA

[4] Professors, Department of Civil, Architectural and Environmental Engineering, Drexel University, Philadelphia, PA 19104, USA

ABSTRACT

Drexel researchers are currently conducting experiments to determine the mechanical behavior characteristics of hollow and fully grouted concrete masonry assemblages, as part of a project funded by the National Science Foundation involving Drexel University, University of Minnesota and University of California-San Diego. The ultimate goal of this study is to thoroughly investigate system-level seismic performance and improve design provisions of partially grouted reinforced masonry buildings.

This paper presents preliminary results regarding full surface displacement and strain fields extracted using the Digital Image Correlation (DIC) technique. DIC, which is a non-contact optical metrology and a non-destructive evaluation method, has been implemented and cross-validated on hollow and fully grouted concrete masonry specimens subjected to axial, bed joint shear and diagonal tension loading. The presented investigation intends to evaluate advantages and challenges of this approach. The obtained DIC data from this research can provide high resolution and full field in-plane and out-of-plane displacements depending on the testing configuration. Global strain measurements as well as strain concentrations can be extracted and DIC is capable to predict crack initiation sites and in-situ monitor the evolution of dominant damage mechanisms.

KEYWORDS: masonry assemblages, digital image correlation, bed joint shear, failure mechanisms

INTRODUCTION

Deformation measurements of concrete masonry walls (CMW) are being performed at Drexel University as part of an on-going research effort funded by the National Science Foundation. The research is motivated by the need to provide design guidelines for partially grouted masonry buildings in moderately seismic regions. The research effort consists of a significant number of experimental tests performed on concrete masonry assemblages and walls loaded to failure. Due to their heterogeneous nature, CMW have a complex fracture behaviour that is difficult to accurately quantify and model. To obtain full field information of the failure processes activated

on CMW, the application of a robust full field surface deformation measurement method named Digital Image Correlation (DIC) is being investigated by Drexel researchers. In addition to traditional deformation and stain measurement techniques, such as LVDTs and strain gauges, a number of non-destructive methods have been used to: (i) monitor deformation during masonry wall tests, for example by using laser interferometry [1] and stereoimaging [2], (ii) to observe crack growth (using e.g. acoustic emission [3]) or iii) to detect/image defects using ultrasounds and computerized tomography [4]. The challenges associated with the usage of such methods include the issue of high sensitivity to vibrations caused by the testing machines, as well as low measuring accuracy and laborious post-processing.

Digital Image Correlation (DIC) is an optical method capable to quantity 2D/3D surface deformation of test specimens and structural components [5, 6]. In DIC, images are captured, processed and stored through a dedicated Data Acquisition System. The image correlation is based on the comparison of an undeformed (reference) image with subsequently recorded "deformed" images. The method is based on tracking typically random speckle patterns applied to the surface of interest by appropriate patterning techniques (spray painting, cotton swab, stencil, speckle patterning, air brush, etc.) and by applying the principles of photogrammetry, digital image processing and stereo imaging [7, 8]. DIC measurements are calibrated for each field of view using NIST-traceable calibration panels that establish coordinate system of axes. A fundamental assumption made in DIC is that the light intensity field defined from surface observations as a digital grayscale remains point-wise unchanged during deformation. Several image correlation algorithms have been developed over the past decades based on which two main categories of DIC methods have been defined: subset [9] and global methods [10]. Displacements in the subset (aka facet) method, which is the one used in this paper, are computed for the centre points of each subset defined around each identified speckle, while there is no enforcement of displacement continuity, which typically leads to noisy fields that require additional smoothing techniques to increase the accuracy of DIC measurements. To address these issues, global (e.g. b-spline interpolation) and finite-element approaches that use nodes instead of subsets have been developed [8]. DIC has great potential as an independent NDT system for SHM, while due to its full field outputs it can additionally cross-validate other NDT techniques such as Acoustic Emission, as well as other metrology devices e.g. strain gages [16].

DIC has been established theoretically and experimentally by several researchers. Chu et al [9] developed a measurement technique by combining deformation theory and digital image correlation method. Luo et al [11] assembled and used a stereo pair of CCD cameras to measure three-dimensional surface-displacement on a cantilever beam and a compact-tension (CT) fracture specimen. Sutton et al. [12] evaluated the feasibility of determining displacement gradients from measured surface-displacement fields and proposed an improved methodology for both the estimation and elimination of noise. Bruck et al. [13] applied Newton-Raphson technique to determined displacements and displacement gradients. They also reported the accuracy of the displacements and displacement gradients for various subset sizes. Peters et al. [14] developed a computer based stress analysis combining digital image correlation of speckle images with an experimental boundary integral method and demonstrated the method on a plate in uniform tension. Choi and Shah observed non-uniform displacement in the displacement contour maps taken at various loading stages on concrete surface using a full-field DIC measuring system [15]. They also illustrated the crack propagation around aggregate interfaces

in their study. The authors have also utilized the theory of DIC to monitor crack growth in aluminum alloys. The DIC results revealed strain concentrations around the crack tip prior to crack extension and cross-validated the results obtained with other non-destructive methods [16]. Corr et al. used DIC to examine interfacial bonding between carbon fiber reinforced polymers (CFRP) and concrete substrates [17]. They analysed the bond constitutive laws and studied the fracture behaviour using these DIC results. Helm et al. [18] developed an improved 3D image correlation system which they tested successfully to measure bending and local buckling behaviour of clamped circular plates under pressure. They measured the surface profile and full-field displacement under the pressure and tension loading with micron level accuracy using their equipment. Digital image processing has been also used to measure dynamic displacement of a structure. Choi et al. [19] introduced a dynamic displacement vision system (DDVS) to measure the dynamic displacement of the masonry structure and a two-story steel frame structure under seismic loading. They compared their DDVS displacement measurement with LVDT results where the percentage of error was 0.471%. A similar application was performed by Lee and Shinozuka to get real-time displacement of a suspension bridge by means of digital image processing technique [20].

Although several studies have been conducted based on the use of DIC, the application of the method to monitor the full field deformation behavior of CMWs has not been yet explored. To this aim, this paper presents an experimental investigation targeting surface strain and displacement contour measurements, shear behavior quantification and progressive damage identification of CMWs.

EXPERIMENTS

A total of three pairs of concrete masonry specimens (CMS) were tested. Each pair consisted of one grouted and one ungrouted (hollow) specimen. Three types of load tests, including (a) compression, (b) shear and (c) diagonal compression tests were carried out. The test setup associated with the different loading scenarios and the corresponding DIC instrumentation is discussed in detail in the following sections.

Compression test of block prisms:

Three unit high prisms were tested under axial compression. An MTS 1556kN capacity actuator mounted on a reacting steel frame was used to apply the vertical axial load. The hollow prisms tested consisted of concrete blocks with nominal size of 200x200x400mm. The half grouted prism contained 200x200x200mm concrete blocks. The experiment was performed with the specified equipment and procedure as described in ASTM C1314. A high slump mixture of cementitious materials, aggregate and water was used to obtain the grout for masonry construction [21]. The grout was prepared according to ASTM C476 requirements and was used to fill the cells of hollow masonry units. An identical grout mixture was used for the remaining tests. Type 5 mortar was used in the construction of test specimen. For axial compression of block prism test, the end plate restraint depends on the prism height. In this experiment, the prism was tested between steel plates and brush platens [Fig. 1]. Strain Gage Sensors manufactured by TML Tokyo Sokki Kenkyujo Co. (named TML sensors in the following) were placed at the backside of the specimen [Fig. 1(a)]. A nominal gage length of 406mm was considered. The speckle pattern needed for DIC measurements was applied on the front side of

the specimens. Fig. 1(b) shows the speckle pattern applied on a pristine half grouted three unit high prism.

Figure 1: Axial compression tests of block prisms: a) Hollow specimen b) Half grouted specimen.

Shear tests:

Shear strength along mortar bed joints was subsequently evaluated. A modified triplet configuration was considered for this experiment [Fig. 2]. A gap was introduced in between the two centre vertical blocks and compressive force was applied through the 1556 kN capacity MTS actuator. Steel plates at both sides were installed to allow stress distribution. The line gauge considered and sketched in Fig. 2 was 406 mm long for the grouted specimen and 373 mm for hollow specimens. The gauge length considered matched the corresponding length of TML gages mounted on the opposite face and not visible in Fig. 2. The gauge length can be assumed between any set of points captured by the DIC images.

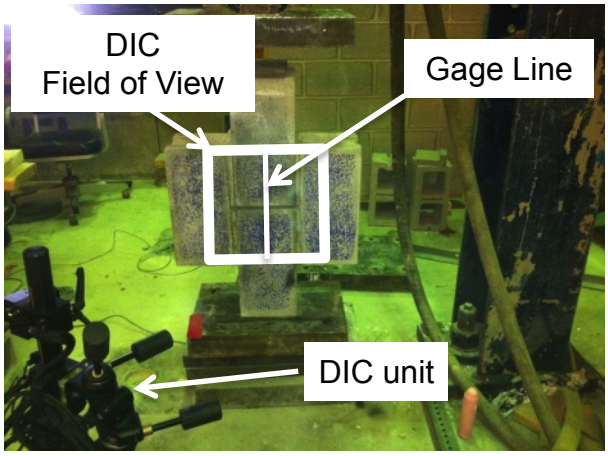

Figure 2: Shear test setup for Hollow specimen; DIC Field of view considered and line gauge for comparison with TML measurements.

Diagonal compression tests:

The last set of tests was performed on 4ft square sections of wall subject to diagonal compression through steel shoes according to ASTM E519. These test specimens were used to determine diagonal tensile strength of masonry specimens (Fig. 3). The specimens were assembled concrete blocks, mortar and grout materials used for axial compression and shear tests. TML gauges were placed along the loading vertical direction and along the horizontal direction on both hollow and grouted samples. It should be noted that the DIC field of view (sketched in Fig. 3a) was restricted to a region of 609x609 mm due to the length of the mounting bar of the DIC system shown in Fig. 3a. As a consequence, no direct comparison was possible between the estimated DIC strain (gauge length ~609 mm) and the elongation measured by the TML gages covering the entire length of the wall diagonal (gage length >1219 mm). Equipment recently purchased and now available at Drexel currently allows a 3657 x 4877 mm field of view and will be soon used to test large walls.

Figure 3: Diagonal compression tests: a) Hollow specimen and b) Grouted Specimen.

DIC Setup:

The digital image correlation (DIC) system used is a GOM Aramis 3D 5 megapixel Camera system containing two Baumer TGX15 cameras with peak acquisition frequency of 30Hz for 3D measurements. Testing parameters such as field of view (FOV), object distance and camera angle were approximately 500x400 mm, 780 mm and 23° respectively. These parameters were optimized using tables provided by the manufacturer and a dedicated calibration block. Distance between two lenses was 308mm. A random speckle pattern was created on the surface by means of a rubber stamp pad. Few pre-test images of the sample were taken to determine the system's sensitivity. The sampling rate was 1~2 frames per second depending on the overall duration of each test. The noise level for strain measurement was approximately 30μm/m. A facet size of 25 x 25 pixels with a step size of 13 pixels was utilized to compute the results.

RESULTS AND DISCUSSIONS:

Full field strain patterns were recorded using the above DIC system for each experiment. While up to 500 snapshots were collected during each test, only images showing the measured full field strain contours near failure are presented here for the sake of brevity. Fig.4(b) shows an example of splitting failure observed in the axially compressed hollow prism. The colour map illustrates the horizontal "x" strain component. It should be noted that large deformations were observed at incipient failure states along the vertical crack visible in the overlapped picture. Fig. 4(b) represents the comparison between the stress-strain curves where the strain was extracted using both the DIC and TML gauges. The strain visualizations corresponding to three stages along the stress-strain curve are shown in Fig. 4(a). It should be noted that although carefully executed, the axial compression test can suffer from eccentricity inducing an uneven strain distribution in the front and back surfaces. A similar trend was observed for the axial compression test of the grouted half prism shown in Fig. 5. The full field strain visualization just prior to final fracture is shown in Fig. 5(b). Again, DIC strain readings were consistently larger compared with the TML strain measurements. These differences could be the consequence of a slight eccentricity inducing a systematic larger deformation on the surface where DIC pattern was applied. Furthermore, it should be pointed out that the DIC estimated strain is evaluated considering 2 points at the ends of the virtual gauge that "mirrors" the TML gage.

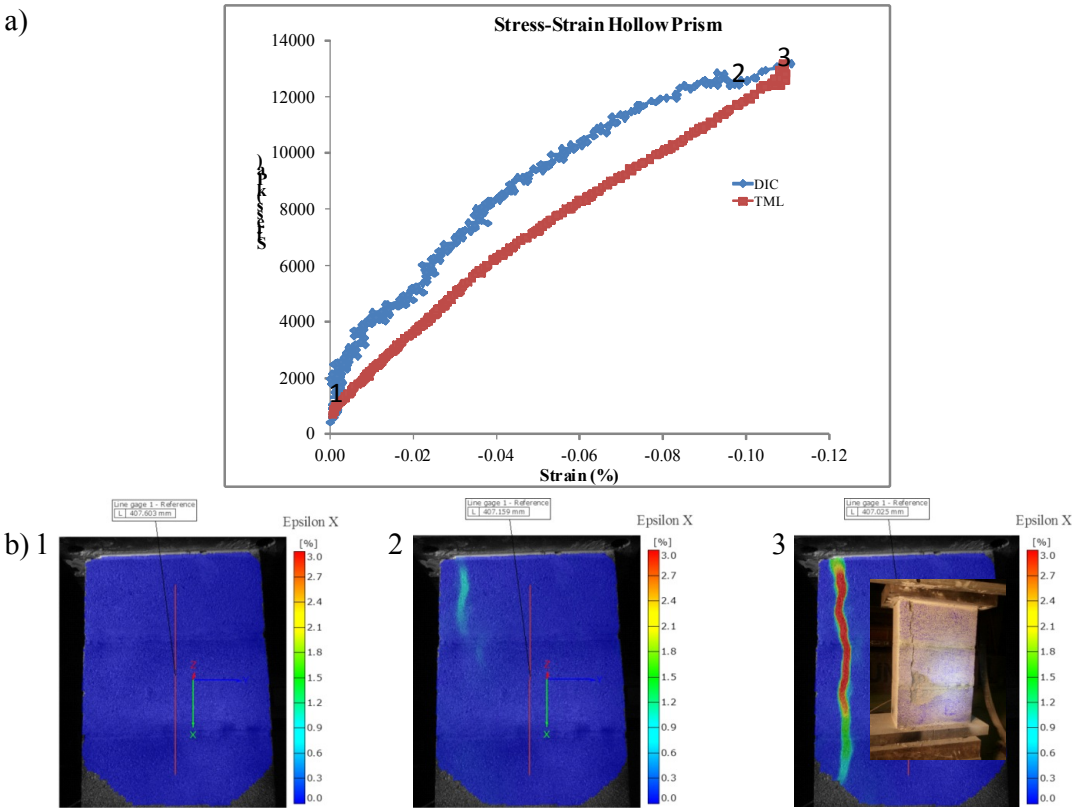

Figure 4: Compression test results for hollow specimen: a) Stress-strain curve comparison between DIC and TML gage (placed along the y direction) b) DIC Strain contour at incipient failure and picture of failed specimen.

Figure 5: Compression test results for grouted specimen: a) DIC Strain contour at incipient failure and picture of failed specimen; b) Stress-strain curve comparison between DIC and TML gage (placed along the y direction).

The next sets of results shown refer to the shear tests. The test set-up of the modified triplet test method was previously illustrated in Fig.2. The DIC field of view included an area of approximately 406 x 406 mm. Strain plots are shown in Figures 6(a) and 7(a) respectively. For both hollow and grouted specimens, higher strain values were observed at the bed joints along the interface between mortar and block at incipient failure states.

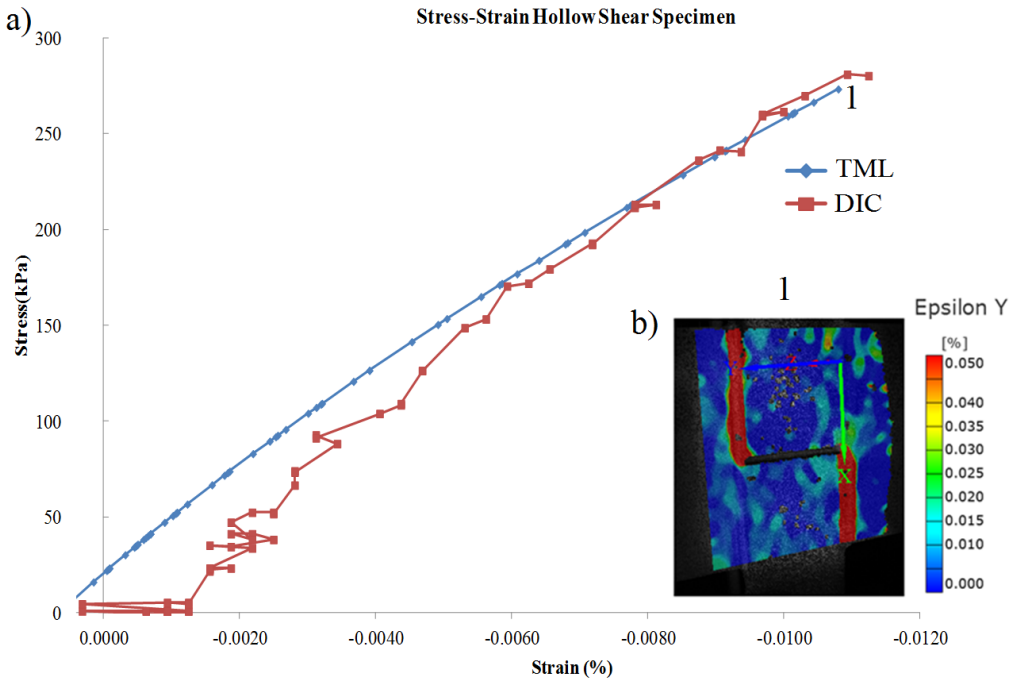

Figure 6: Shear test results for hollow specimen: a) Stress-strain curve comparison between DIC and TML gage b) DIC Strain contour at failure.

Hollow and grouted samples exhibited a large strain along the bed joints [Fig. 6 and Fig. 7] and as expected, failure occurred by shear slip along the same critical planes. While the grouted

Figure 7: Shear test results for grouted specimen: a) Stress-strain curve comparison between DIC and TML gage b) DIC Strain contour at failure; DIC virtual gauge is the dotted line along the y direction.

specimen failed in a very similar manner, some cracks developed throughout the blocks. As expected, the ultimate shear stress of the hollow triplet specimen was lower than the grouted one where the grout is continuous through the hollow cells. The measured shear capacities of the hollow and grouted specimens were 289.5 kPa and 579 kPa respectively. Again, the comparison between strain estimated by the presented DIC approach and the TML reading was satisfactory. For the hollow specimen, the maximum strain measured at failure was less than 150microstrains.

The final set of tests performed was the diagonal compression test [Fig. 3]. Two assemblages were again considered (i.e. hollow and grouted). Fig. 8 shows the results obtained for the hollow wall, while Fig. 9 summarizes the results obtained for the grouted wall. A DIC field of view of 406 x 406 mm was considered. The strain contour at incipient failure captured by the DIC approach is depicted in Fig. 8(a). A noise of approximately 50microstrain was observed during DIC measurements and it is visible in Fig. 8(a). Time averaging can minimize reading oscillations (see curve DIC smooth). The strain accumulation along the bed joints is obvious. Failure, as expected, occurred along these weak planes. The failed wall is shown in the same Fig. 8(a). The maximum strain measured during the test by the TML gage (with a gage length exceeding 1219 mm was significantly smaller if compared to the strain estimated using the DIC [Fig. 8(b)]. However, the small field of view of the DIC restricted the gauge length to about 508 mm. Consequently, a “true” comparison between TML gage and DIC was not possible. The stress vs strain curves obtained for the diagonal compression test of the hollow specimen is shown in Fig. 8(b). It can be noted that the maximum stress measured was estimated to be about 965.2 kPa.

A comparison between DIC and TML gage was not possible for the grouted wall due to a malfunctioning of the TML gage. However, Fig. 9(a) clearly shows again the capability of the DIC to identify the regions with strain concentration and therefore with the locations where

failure eventually occurs. A picture of the wall after the complete failure is shown in Fig. 9(a). Since grout-filled cells tend to reinforce the mortar joints, the cracks do not clearly form along the mortar but locally extend through the units.

Figure 8: Diagonal compression test for hollow specimen: a) Stress-strain curve comparison between DIC and TML gage b) DIC Strain contour at incipient failure; two DIC virtual gages are placed in the x and y directions

Figure 9: Diagonal compression test for grouted specimen: a) Photo of the failed grouted assemblage; b) DIC Strain contour at incipient failure; two DIC virtual gages are placed in the x and y directions; b) Stress-strain curve comparison between DIC and TML gage.

CONCLUSION:

The DIC method has been successfully implemented to determine non-uniform strain contours on several concrete masonry assemblages estimating their surface deformation. This system has been verified by comparing strain along selected directions with traditional TML gauge results. In addition to monitoring the strain across the gage length, the DIC provided full field strain behavior and often revealed strain hot-spots at locations that corresponded to failure. The DIC system demonstrated impressive potential for stress-strain monitoring. The ability to characterize and anticipate failure mechanisms of concrete masonry systems at different testing conditions was also shown. Some challenges that are currently investigated are a) the need for a larger field of view and b) the use of filtering techniques to decrease the noise level in the strain measurements. Drexel researchers are currently preparing to test a large wall where a DIC field of view of 3658 x 3658 mm will be employed allowing for a full field investigation of failure .

ACKNOWLEDGEMENTS

This research is supported by the National Science Foundation under the Network for Earthquake Engineering Simulation program with Award No.CMMI-1208208. Partial support from the National Concrete Masonry Association is also gratefully acknowledged. The support of Delaware Valley Masonry Institute and Sabia Mason Contractors in providing the mason to build the test specimens is acknowledged. However, opinions expressed in this paper are those of the authors and do not necessarily reflect the opinions of the sponsors.

REFERENCES

1. Binda L., Facchini M., Roberti G. Mirabella, Tiraboschi C. (1998) "Electronic speckle interferometry for the deformation measurement in masonry testing", Construction and Building Materials 12 _1998. 269281
2. She A. C., Hjelmstad K. D.,Huang T. S. (1992) "Structural damage detection using stereo camera measurements" Nondestructive Evaluation of Civil Structures and Materials, p. 345-356
3. Carpinteri A., Lacidogna G. (2006) "Damage monitoring of an historical masonry building by the acoustic emission technique" Materials and Structures 39:161–167
4. Popovics J S (2003)"NDE techniques for concrete and masonry structures" Prog. Struct. Engng Mater; 5:49–59 (DOI: 10.1002/pse.146)
5. Sutton M A, Walters W J, Peters W H, Ranson W F and McNeil1 S R,(1983) Determination of displacements using an improved digital correlation method. Image and Vision Computing,. **1**(3): p. 133-139.
6. Sutton, M.A., J.J. Orteu, and H.W. Schreier, Image Correlation for Shape,(2009) Motion and Deformation Measurements: Basic Concepts, Theory and Applications: Springer.
7. Pan, B., et al., (2009) Two-dimensional digital image correlation for in-plane displacement and strain measurement: a review. Measurement Science and Technology,. 20(6): p. 062001-062001.
8. Cofaru, C., W. Philips, and W. Van Paepegem, (2010) "Improved Newton-Raphson digital image correlation method for full-field displacement and strain calculation." Applied optics,. 49(33): p. 6472-84.
9. Chu, T.C., Ranson, W.E, Sutton, M.A. and Peters, W.H., (1985) "Applications of Digital-image-correlation Techniques to Experimental Mechanics," Experimental mechanics, 25 (3), 232-244.
10. Sun, Y., et al., Finite element formulation for a digital image correlation method (2005). Applied Optics,. 44(34): p. 7357-7363.
11. Luo, P.F., Chao, YJ., Sutton, M.A. and Peters, W.IL I11, (1993) "Accurate Measurement of Three-dimensional Deformations in Deformable and Rigid Bodies Using Computer Vision," Experimental mechanics, 33 123-132.
12. Sutton, M.A., Turner, J.L., Bruck, H.A. and Chae, T.A., (1991) "Full-field Representation of Discretely Sampled Surface Deformation for Displacement and Strain Analysis," Experimental mechanics, 31 (2), 168-177
13. Bruck, H.A., McNeill, S.R., Sutton, M.A. and Peters, W..H. 111, (1989) "Digital lmage Correlation Using Newton-Raphson Method of Partial Differential Correlation," Experimental mechanics, 28 (3), 261-267.
14. Peters, W.H. and Ranson, W.F., (1982) "Digital Imaging Techniques in Experimental Stress Analysis," OPT. ENG., 21 (3), 427-431

15. Choi, S. and Shah, S.P. (1997). “Deformation measurement in concrete under compression using image correlation,” Journal of experimental mechanics 37(3), 307–313.
16. Vanniamparambil P.A., Bartoli I., Hazeli K., Cuadra J., Schwartz E., Saralaya R., Kontsos A. (2012) “An Integrated SHM Approach for Crack Growth Monitoring,” Journal of intelligent material systems and structures, 23(14), 1563–1573.
17. Corr D., Accardi M., Brady L., Shah S. (2006) “Digital image correlation analysis of interfacial debonding properties and fracture behavior in concrete,” Engineering fracture mechanics 74 (2007) 109–121
18. Helm J.D., McNeill S.R., Sutton M.A. (1996) “Improved three-dimensional image correlation for surface displacement measurement,” OPT. ENG. 35(7) 1911–1920.
19. Choi H.S., Cheunga J.H., Kimb S.H., Ahn J.H. (2011) “Structural dynamic displacement vision system using digital image processing,” NDT&E international 44 (2011) 597–608
20. Lee J.J., Shinozuka M. (2006) “Real-Time Displacement Measurement of a Flexible Bridge Using Digital Image Processing Techniques,” Experimental mechanics 46: 105–114
21. Drysdale R.G., Hamid A.A. (2008), “Masonry structure behaviour and design,” The masonry society, ISBN 1-99081-33-2